water

MDPI

Article

Hydrological Analysis of the 2024 Flood in the Upper Biała Lądecka Sub-Basin in South Poland

Jakub Izydorski * and Oscar Herrera-Granados

Faculty of Civil Engineering, Wrocław University of Science and Technology, Wyb. Wyspiańskiego 27, 50-370 Wrocław, Poland; oscar.herrera-granados@pwr.edu.pl
* Correspondence: jakub.izydorski@pwr.edu.pl

Abstract

The SCS-CN (Soil Conservation Service Curve Number) model is important for flood forecasting as it provides a relatively simple and widely used methodology for estimating the amount of surface runoff from a rainfall event, which is a crucial input in predicting flood volumes and peaks in ungauged or data-scarce watersheds. Thus, the authors developed a hydrological model based on the SCS-CN curve methodology and GIS (Geographic Information Systems) to estimate the flood hydrograph in the upper parts of the Biała Lądecka River basin in Poland. The numerical model was calibrated based on the data available from the Polish Institute of Meteorology and Water Management (IMGW). The output of the model demonstrates the effect in the flood hydrograph at the town of Lądek-Zdrój. Additionally, hydraulic routing calculations were included to analyze the possible causes of the dam failure of the Stronie Śląskie reservoir in the year 2024. The main purpose of this study is to corroborate the influence of climate change on flood events and their consequences, as well as to assist in forecasting future catastrophic hydrological events and thus earlier adaptation and reinforce the infrastructure in our territories against future flooding.

Keywords: SCS-CN curve methodology; Geographic Information Systems; reservoir routing; hydraulic routing; model development

check for updates

Academic Editors: Athanasios Loukas and Aikaterini Lyra

Received: 12 November 2025
Revised: 11 December 2025
Accepted: 14 December 2025
Published: 18 December 2025

Citation: Izydorski, J.; Herrera-Granados, O. Hydrological Analysis of the 2024 Flood in the Upper Biała Lądecka Sub-Basin in South Poland. *Water* **2025**, *17*, 3593. https://doi.org/10.3390/w17243593

Copyright: © 2025 by the authors. Licensee MDPI, Basel, Switzerland. This article is an open access article distributed under the terms and conditions of the Creative Commons Attribution (CC BY) license (https://creativecommons.org/licenses/by/4.0/).

1. Introduction

1.1. The Flood of September 2024

The year 2024 witnessed a series of unprecedented flood events throughout Europe, which required a re-evaluation of established hydrological analysis methods. In September 2024, the "Boris" storm system brought intense rainfall to Central Europe, affecting countries such as Austria, Czechia, Romania, Slovakia, and Poland. The Kłodzko Valley (South Poland) has experienced several catastrophic floods throughout its history, with two major events in recent decades: July 1997 (the so-called "Millennium Flood") and September 2024. Historical records also mention severe floods in 1783, 1888, and 1938, which caused significant damage to infrastructure and settlements along the Nysa Kłodzka River [1]. The 2024 flood event caused significant damage within the Biała Lądecka and Nysa Kłodzka river basins. The destruction ranged from catastrophic damage to buildings, destroying historic bridges like St. John's (Lądek-Zdrój), cutting off water/roads, and displacing residents to halting local services, necessitating long-term infrastructure repair and psychosocial support in the heavily impacted Kłodzko Valley region of Poland [2]. In the case of the Biała Lądecka basin, two stream gauge stations recorded the hydrograph during

the flood events. However, in the case of the station located in the town of Lądek-Zdrój, there is an information gap of around 34 h (between 15 and 16 September of 2024). The SCS-CN method is widely used to estimate the runoff in mountainous catchments due to its simplicity and minimal data requirements, making it especially useful in ungauged or data-scarce regions [3]. Hence, in this contribution, the authors try to forecast this gap. To fill this gap and acquire a deeper understanding of the flood's impact, a numerical model was developed based on the SCS-CN method. This model provides crucial information on the hydrological behavior of the basin. The authors anticipate that this model will serve as a valuable tool for future planning and mitigation strategies, helping decision-makers to address the growing effects of climate change.

1.2. Case Study: The Upper Biała Lądecka Basin

In September 2024, storm Boris hit Central Europe, bringing intense rainfall in many countries such as Austria, Czechia, Romania, Slovakia, and Poland. These rainfall events in South Poland caused widespread damage in the basins of the Biała Lądecka and Nysa Kłodzka rivers. A catastrophe occurred in this basin as one of the earth embankments that formed the flood detention reservoir located in the Morawka river vanished due to heavy rainfall (see Figure 1).



Figure 1. The Stronie Śląskie reservoir and its outlet elements after the catastrophe. View from upstream.

From 11 to 16 September 2024, within the the Biała Lądecka catchment area, significant rainfall occurred, and data were collected from local meteorological stations (depicted in Figure 2). The rainfall began as a light shower on the afternoon of 11 September, with hourly rates under 0.2 mm. The precipitation became practically continuous from 5:00 a.m. UTC on 12 September, lasting until the late evening of 16 September. The heaviest downpour occurred from 14 to 15 September, with some stations recording up to 23.8 mm of rain per hour. Unfortunately, due to the intense precipitation or other technical issues, several stations failed to collect data on 15 and 16 September.

The authors investigated how rainfall data affect runoff transformations, examining two scenarios: in the first, it was assumed that rainfall was fully recorded at the Śnieżnik meteorological station; while in the second, rainfall was interpolated for each catchment using the IDW method. The IDW method was chosen as it is easy to apply and the results obtained are consistent and logical. Moreover, the IDW method is considered as a valid method for rainfall estimation [4,5].

For these scenarios, two conditions were analyzed: one where the Stronie Śląskie Dam does not exist and another where the Stronie Śląskie Dam did not experience failure. The

map of the case study is depicted in Figure 2. As shown, six sub-basins can be identified: (1) West Morawka; (2) Kamienica-Bolesławów; (3) the Stronie Śląskie reservoir influential area; (4) Stary Gierałtów; (5) the River Morawka outlet; and (6) the upper basin.

For our case study, analyzing the hydraulic capacity of the Stronie Śląskie reservoir (located in sub-basin 3) is very important due to the fact that the failure of this detention reservoir was the main reason for the catastrophic consequences of the 2024 flood in several towns such as Lądek-Zdrój or Żelazno.

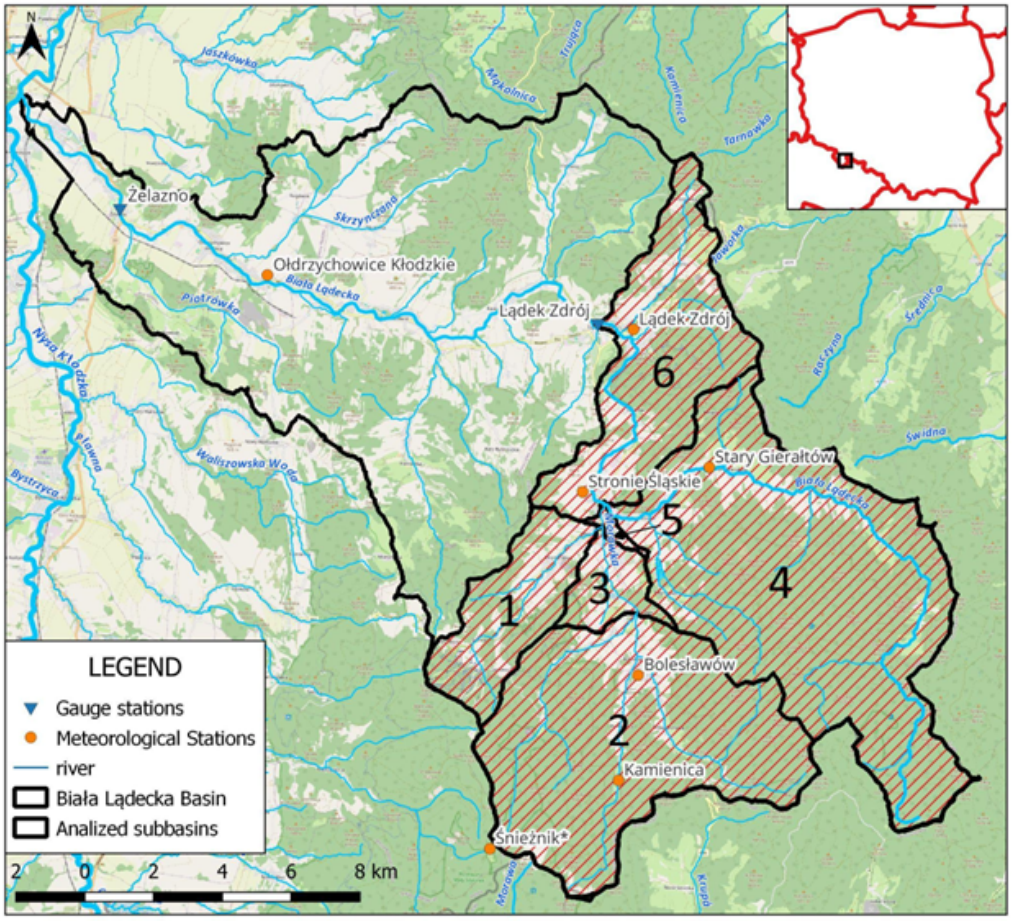


Figure 2. The case study location area in South Poland. The map in the upper-right corner indicates the location of the case study within the country (black square).

Therefore, in this contribution, the authors focused on analyzing the hydraulic conditions and operations of the flood relief structures (spillways and culverts) of the reservoir under maximal capacity conditions. The reservoir was provided with three relief structures, namely, (i) the culverts in the lower part of the main structure; (ii) the arch tunnel located in the middle of the concrete dam (around 7 m from the river bed); and (iii) the main spillway of the concrete structure located around one meter below the crown of the earth dyke.

1.3. Hydrological Models for Flood Analysis

There are many types of rainfall–runoff model, including physical, conceptual, and empirical [6]. The Green–Ampt infiltration model [7]—and various modifications and extensions thereof—is an example of a physical and conceptual model that is used widely for analyzing the relationships between rainfall, infiltration and runoff for a range of conditions and from different theoretical and experimental perspectives (Ahuja and Ross, 1983 [8]; Barry et al., 2005 [9]; Basha, 2011 [10]; Bouwer, 1978 [11]; Chen and Young, 2006 [12]; Gowdish and Muñoz-Carpena, 2009 [13]; Hilpert and

Glantz, 2013 [14]; Hogarth et al., 2013 [15]; Mein and Larson, 1973 [16]; Parlange et al., 1982 [17]; Voller, 2011 [18]; Chen, Li, et al., 2015 [19]; among others). But in this case, probably the most popular and simple-to-use empirical SCS-CN method was applied.

This method is the result of extensive field investigations carried out during the late 1930s and early 1940s and the work of several early researchers, including Mockus (1949) [20], Sherman (1949) [21], Andrews (1954) [22], and Ogrosky (1956) [23]. The primary reason for its wide applicability and acceptability lies in the fact that it accounts for most runoff-producing watershed characteristics: soil type, land use/treatment, surface condition, and previous moisture condition [24]. In addition, it is very useful for ungauged watersheds.

In this study, the following rainfall-and model was applied (Equation (1)).

$$P = I_a + F + Q \quad (1)$$

where P is the total rainfall; I_a is the initial precipitation loss before the onset of runoff; F is the cumulative infiltration, including I_a; and Q is the direct runoff. The initial precipitation can be estimated using Equation (2):

$$I_a = \lambda \cdot S \quad (2)$$

where λ is a regional parameter dependent on geological and climatic factors ($\lambda \ \epsilon$ (0; 0.2 ÷ 0.3)); and S is the potential maximum retention or infiltration. The first parameter is usually initially set to lambda = 0.2, but scientists have questioned this value, claiming on the basis of research that it is too high, especially for mountainous regions. Instead, they suggest setting lambda = 0.05 [25]. The latter parameter was determined by the SCS-CN model (Equation (3)).

$$S = 1000/CN - 10 \quad (3)$$

where CN (Curve Number) represents a numerical factor that reflects the ability of the soil to retain water ($CN \ \epsilon$ (0 to 100)). It depends on the type of soil, the type of vegetation cover, the treatment of the ore used on the land, the hydrological condition, the antecedent moisture condition, and the climate of the watershed [24].

2. Materials and Methods

2.1. GIS Support for Hydrological Analysis

In this analysis, GIS (Geographical Information Systems) support is invaluable. GIS play a crucial role in hydrological analysis by providing powerful tools for spatial data management, visualization, and modeling. Moreover, GIS allow for spatial data integration; hydrological processes are inherently spatial—rainfall, runoff, infiltration, and evapotranspiration vary across landscapes. GIS allow integration of diverse datasets, as follows: (i) Digital Elevation Models (DEMs); (ii) land use/land cover maps; (iii) soil types; (iv) climate data; and (v) hydrography (rivers, lakes, watersheds). Table 1 displays the most important data that was used for the analysis and its source of retrieval.

GIS also allow watershed and stream network delineation using terrain data. This process was carried out by the authors using the GIS tools included within the HEC-HMS 4.13 beta.6 software [26]. In Figure 3, the process of the determination of the sub-basins that were analyzed in this contribution is depicted: (A) flow direction; (B) identified streams (using Strahler method); (C) flow accumulation; and (D) final delineation and elements used for hydrological modeling. The complete process of the watershed delineation and

stream network identification using GIS is well known and described in the literature, such as in the book by Dixon and Uddameri (2015) [27].

Table 1. Data type that were used for the analysis and their source of information.

Data Type	Source or URL	Accessed Date	Comments
Digital Elevation Model	geoportal.gov.pl	21 October 2024	5 × 5 m resolution
Land cover/land use map	scalgo.com/live	21 October 2024	1 × 1 m resolution
Detailed Geological Map	PIG-PIB	28 October 2024	Scale 1:50,000–2020
Rainfall data	IMGW	14 October 2024	
Discharge (Lądek-Zdrój)	IMGW	14 October 2024	

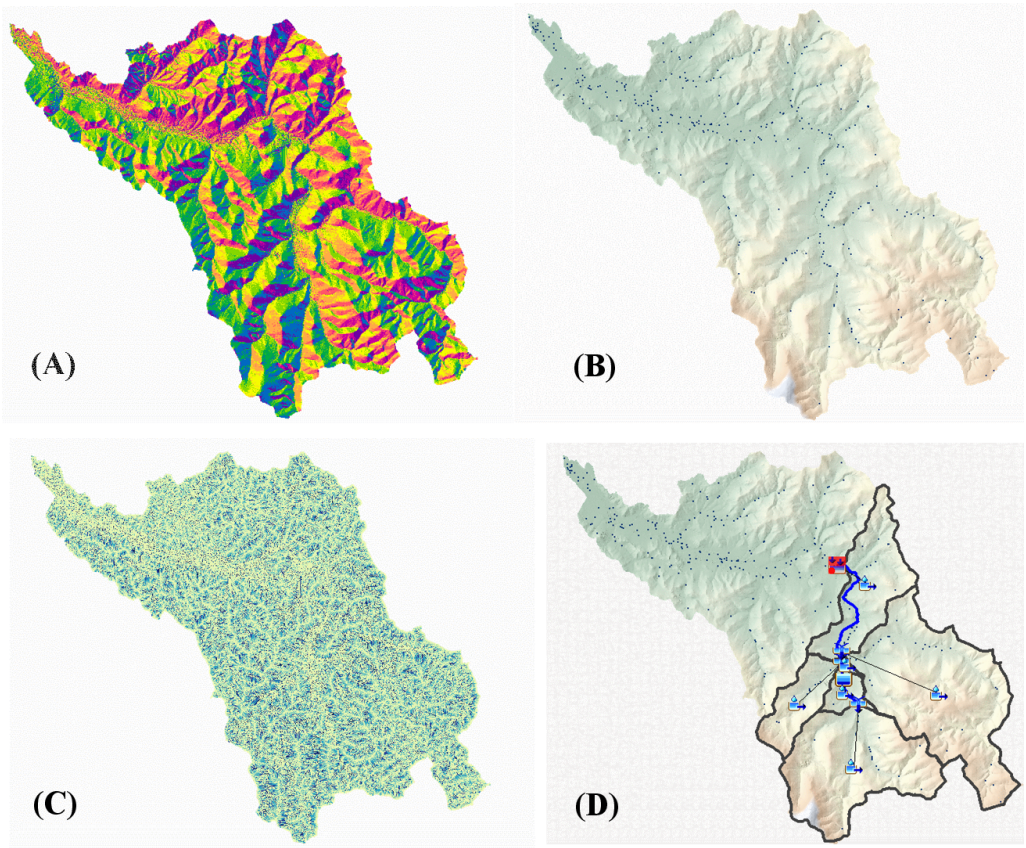


Figure 3. GIS support to build the hydrological model and final geometry.

Spatial analyses were used to determine the percentage distribution of land cover in a given sub-catchment area and the dominant soil type, which are necessary for determining the *CN* (described in further sections). The distribution of precipitation in the catchment area was obtained, the average slope of the catchment area was calculated, and the longest runoff paths were identified. These analyses were carried out using the web-based GIS application SCALGO Live [28] and the open-source software QGIS 3.28.8.

2.2. Essential Data for Hydrological Analyses

The curve number (*CN*) is the key parameter used to model runoff, and its determination relies on two main factors: soil type and land cover. The United States Department of Agriculture (USDA) classifies soils into four Hydrologic Soil Groups (A, B, C, and D) based on their infiltration rate [20]. Group A soils have the highest infiltration rates, while Group D soils have the lowest.

To assess *CN*, understanding the soil type and land cover within the sub-basin is crucial. Soils are categorized by their infiltration rates into four groups (A–D). Group A

soils exhibit high infiltration rates, whereas Group D soils demonstrate low rates. The area of study predominantly consists of gneisses and shales. Alluvial sands, gravels, and clays are located near watercourses but constitute a minor portion of the catchment area. As a result, the sub-basins are mainly classified as Group C and D, with the exception of sub-basin 5, which falls under Group B. The groups was determined using the Detailed Geological Map of Poland at a 1:50,000 scale (Figure 4), which is compiled and provided by the Polish Geological Institute—National Research Institute (PIB, Polish acronym). Table 2 depicts the summary of the *CN* determination for sub-basin 4 (Stary Gierałtów). The *CN* value for a given sub-basin was determined based on the weighted average percentage of the land use surface multiplied by the *CN* value for a given land group. This analysis was carried out for all the six sub-basins identified in the study area (see Figure 2).

Table 2. Land use coverage according to SCALGO and *CN* estimation for sub-basin 4.

Landuse/Land Cover	Hydrologic Condition	Surface (km^2)	Surface (%)	Weighted CN (%)
Building		0.089	0.0013	0.117
Bush/shrubbery	Good	0.038	0.0006	0.044
Forest	Good	54.54	0.8180	57.260
Other constructions		0.073	0.0011	0.108
Grass	Good	9.027	0.1354	9.613
Orchand	Good	0.011	0.0002	0.014
Wetlands		0.003	0.0001	0.010
Industrial/storage area		0.005	0.0001	0.009
Unknown		0.172	0.0026	0.260
Cultivated land	Poor	1.079	0.0162	1.377
Flowing water		0.140	0.0021	0.206
Standing water		0.081	0.0012	0.118
Shopping and service buildings		0.004	0.0001	0.009
Single-family buildings		0.492	0.0074	0.666
Industrial-storage buildings		0.020	0.0003	0.028
Multi-family buildings		0.012	0.0002	0.018
Coppices	Fair	0.029	0.0004	0.023
Woodlet	Fair	0.855	0.0128	0.934

The Biała Lądecka catchment area is primarily composed of gneisses and shales, which have been classified into Hydrologic Soil Groups C and D due to their low infiltration capacity. While alluvial sands, gravels, and clays are present near watercourses, they constitute a small portion of the overall area. An exception to this classification is sub-basin 5, which falls under Group B, indicating a moderate infiltration rate.

To determine the land cover, a detailed analysis was conducted using the SCALGO high-resolution land cover map, which was produced by machine learning techniques, orthophotos, and other input data [28]. Figure 4 illustrates the various land cover types identified within the sub-catchment (upper Biała Lądecka basin).

The HMS model allows us to consider different natural phenomena such as evapotranspiration, snowmelt, water control structures, and others [29]. For the scope of this research (due to the nature of the rainfall event), only four natural phenomena were considered, namely, precipitation (using the recorded hyetographs), runoff volume (using the SCS-CN method), directand (using SCS), and hydraulic routing (using Muskingum and other methods).

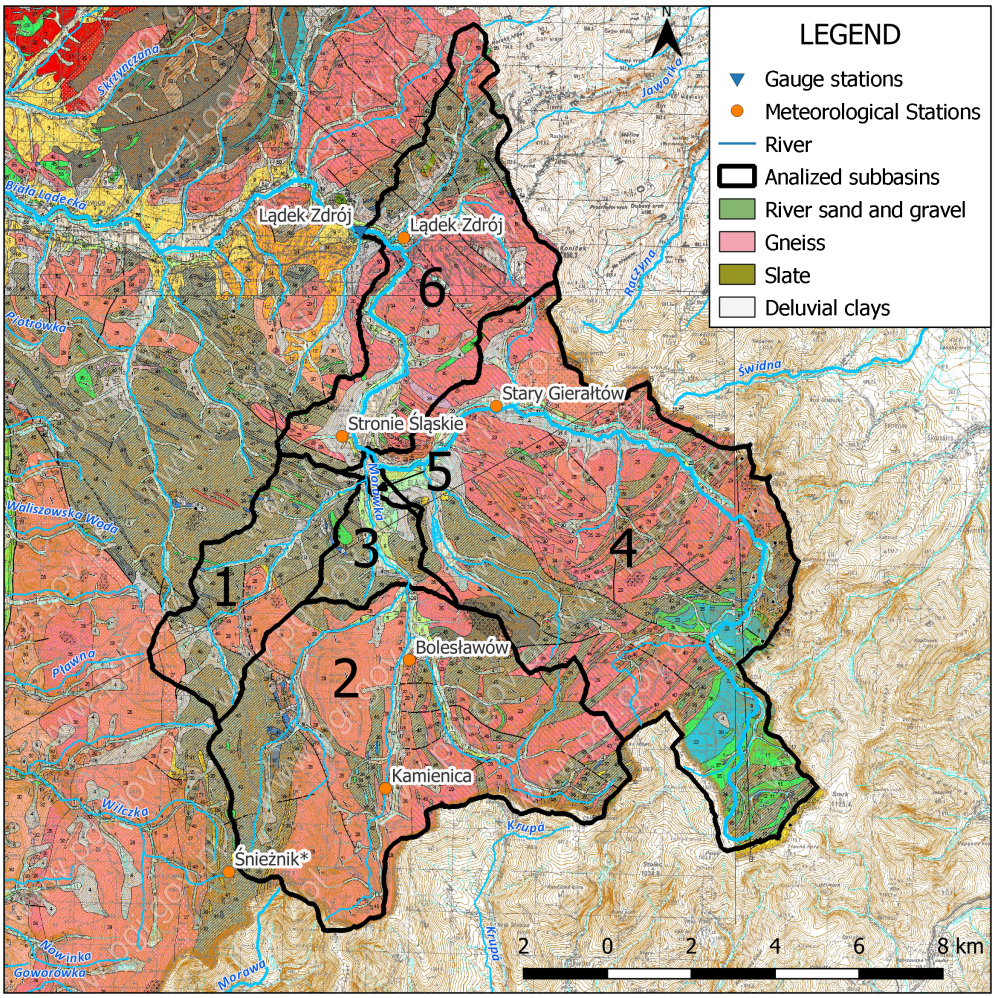


Figure 4. Geological map of the case study area.

2.3. Rainfall Data

GIS data is essential for this study. However, in order to implement a rainfall-runoff model, rainfall data is crucial. Rainfall is the primary source of freshwater in most hydrological systems. The rainfall data was retrieved using the online available information provided by the the Polish Institute of Meteorology and Water Management (IMGW). The data was retrieved using its live webpage [30] and is depicted in Figure 5.

As mentioned in the introduction, in our research, two cases were considered: in the first case, precipitation data from the fully registered Śnieżnik meteorological station, located close to case sub-basin (marked with "*" at Figures 2 and 4), was used for the entire catchment area; and in the second case, data recorded at seven meteorological stations (five of which are located in the studied catchment area) was interpolated using the inverse distance weighted method (see Figure 5). This method is based on the conception of Tobler's first law from 1970 (the first law of geography), i.e., the rule that as everything is connected with everything, but closer objects have a greater influence than more distant ones [4].

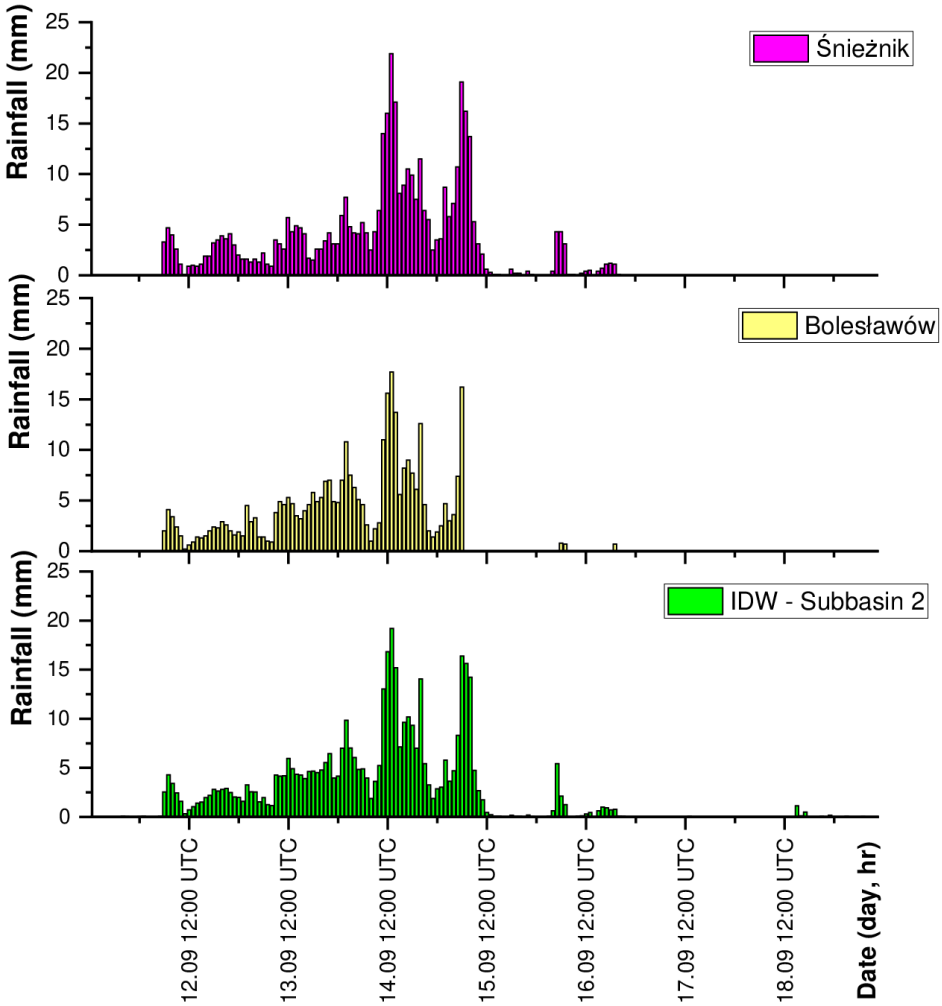


Figure 5. Hyetographs of two meteorological stations and the statistically estimated rainfall.

In the IDW method, the value at the unknown point is calculated as the weighted average of the values of the n-known points. It can therefore be used to estimate unknown precipitation data based on known data from locations adjacent to the unknown location [31–33]. IDW is classified as a deterministic method, which results from the lack of requirement to meet specific statistical assumptions in calculations, which can be considered an advantage. The IDW method can be represented with the following equation [4]:

$$Z(x_0) = \frac{\sum_{i=1}^{n} w_i Z(x_i)}{\sum_{i=1}^{n} w_i} \tag{4}$$

where n is the number of observation points, $Z(x_i)$ is the value at point x_i, and w_i is the weight assigned to each point. The weight is typically calculated based on the inverse of the distance d_i raised to a power p:

$$w_i = \frac{1}{(d_i)^p} \tag{5}$$

A common choice for the power parameter is $p = 2$ (inverse squared weighting). After the interpolation, the average hourly precipitation value was calculated for each sub-basin. The Raster processing algorithm-analysis $\rightarrow$ zonal statistics was used using the QGIS software, where the precipitation data contained in raster files was converted into vector files containing information on average precipitation in each sub-basin. The vector files were then merged, and the attribute table was exported. The hyetograph for the

Śnieżnik station and Bolesławów station (located in sub-basin 2) and interpolated (using IDW method) rainfall data for sub-basin 2 are shown in Figure 5.

2.4. Transform Method

In HEC-HMS, many loss methods and transform methods (e.g., the Clark Unit Hydrograph) for determining runoff are available [26]. In this study, we decided to use the method developed by the same organization who developed the loss method, namely, the SCS Unit Hydrograph, which should ensure conceptual consistency. The relationship between precipitation and runoff is characterized by a parameter known as lag time, which quantifies the delay between a rainfall event and the resulting runoff. As Mishra and Singh [24] note, various definitions and formulas exist for estimating lag time, each with its own specific limitations.

In this study, the Soil Conservation Service (SCS) method was employed, with lag time defined according to Equation (4). The lag time for each catchment was estimated based on two key metrics: the longest runoff path and the average slope. The longest runoff path was determined using SCALGO Live while the average slope was calculated via a Digital Elevation Model (DEM) using GIS tools from QGIS and HEC-HMS, as depicted in Equation (6).

$$t_1 = \frac{l^{0.8}(2540 - 22.86CN)^{0.7}}{14104CN^{0.7}Y^{0.5}} \quad (6)$$

where t_1 is the catchment lag time in hours [h]; l is the longest runoff path [m]; and Y is the average catchment slope [m·m^{-1}]. In Table 3, these parameters are summarized for the six sub-basins. These parameters were determined using GIS algorithms.

Table 3. Summary of parameters (necessary for modeling purposes) of the analyzed sub-basins.

Sub-Basin Name (ID)	Longest Path (m)	Estimated *CN* Value (-)	Average Slope (%)	Average Slope (m/m)	Lag Time (min)
Lądek-Zdrój (6)	10,017.91	71.92	20.56	0.2056	87.04
Stary Gierałtów (4)	27,497.63	70.82	25.69	0.2569	180.01
Outlet Morawka (5)	930.64	72.40	8.20	0.0820	20.33
Western Morawka (1)	9958.46	71.35	24.43	0.2443	80.72
Stronie Śląskie Res. (3)	3590.32	72.60	17.43	0.1743	40.82
Kam-Bolesławów (2)	12,315.85	70.66	30.38	0.3038	87.43

Figure 6 displays the general flowchart of the steps that the authors undertook to set up and run the simulations.

2.5. Routing and Reservoir Routing Using HEC-HMS

When modeling a river or stream in HEC-HMS, we use a reach defined by the stream network delineation. This element sums up inflows from other elements of the catchment model and transforms them into a single outflow (differently from the hydraulic analysis in classical hydraulic models such as HEC-RAS). The outflow is calculated using one of several available methods of open channel flow simulation. In this case, the simple but reliable Muskingum model was applied, employing the principle of mass conservation to trace the inflow hydrograph. It can utilize the hysteresis between outflow and inflow, taking this into account in the simulation to increase and decrease the channel capacity depending on the rise or fall of the flood wave. As an initial condition, three parameters must be specified: K, the travel time of the flood wave through the routing reach (in hours); X, the dimensionless weight and number of subreaches; and the flood wave flow time,

estimated via the relationship between the ratio of the length of the reach L and the flood wave velocity V_w.

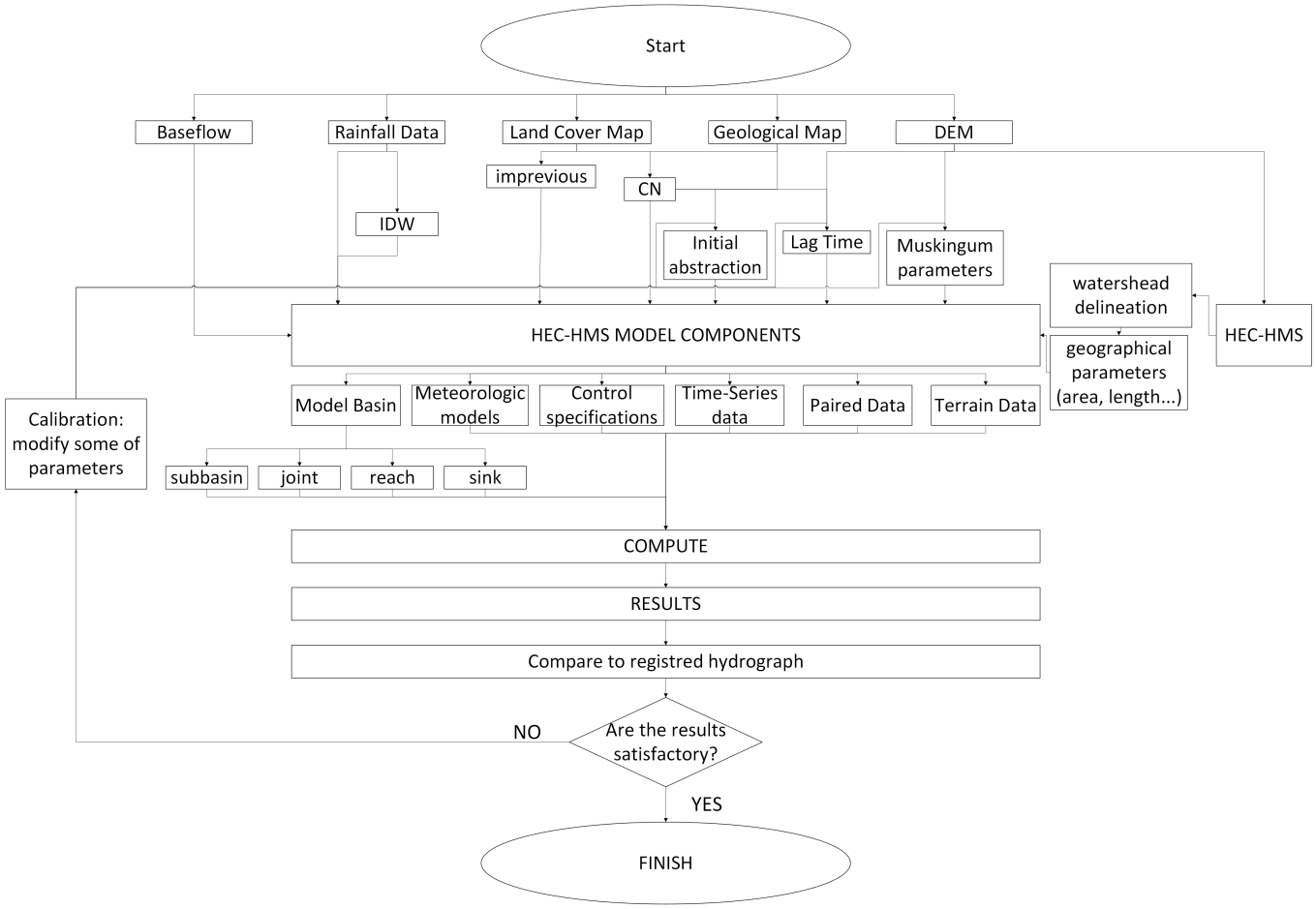


Figure 6. Flowchart displaying the modeling methodology to calculate the flow hydrograph—no reservoir.

The flood wave velocity was estimated based on the river velocity calculated using the well-known Manning's Equation (7) for the cross-sections located in the riverbed, multiplied by the coefficient C_w ranging from 1.33 to 1.6. The attenuation coefficient X does not have a strong physical meaning, and its value ranges from 0.0 to 0.5, where the minimum value indicates maximum attenuation and the maximum value indicates minimum attenuation.

$$V_w = C_w \cdot \frac{1}{n} \cdot {R_h}^{2/3} \cdot {S_o}^{1/2} \tag{7}$$

where R_h is the hydraulic radius in meters, and S_o is the hydraulic gradient.

Suppression will also be affected by the number of sub-basins; the more there are, the closer the attenuation will be to 0. This number can be preliminarily determined based on the following relationship:

$$N = \frac{K}{\Delta t} \tag{8}$$

where K is the travel time of the flood wave through routing reach, and Δt is the simulation time step. The main drawback of the model is that the average velocity of the river varies with its depth, and the damping coefficient is set by trial and error, which is why the Muskingum model parameters were mainly used for calibration.

While a reservoir element in HEC-HMS conceptually represents a natural lake or a lake behind a dam, the actual storage simulation calculations are performed by a routing method in conjunction with a storage method, contained within the reservoir [26].

The "level dam top" method assumes that flow over the dam can be represented as a broad-crested weir. The calculations are essentially the same as for a broad-crested spillway (Equation (9)), but they are included separately for conceptual representation of the reservoir structures.

$$Q = C_d L H^{1.5} \tag{9}$$

where Q is the discharge of the spillway in cubic meters per second; C_d is the Weir coefficient with values that range from 1.5 to 2.6; L is the length of the crest; and H is the head above the crowns in meters. The crest elevation of the dam top must be specified in order to allow for the determination of H.

The length of the dam top L should represent the total width through which water passes, excluding any other amount occupied by spillways. The discharge coefficient accounts for energy losses as water approaches the dam top and flows over the dam. In addition, the *Outflow Structures Routing Method* method was applied for this contribution.

The *Outflow Structures Routing Method* is designed to model reservoirs with a number of uncontrolled (or nominally controlled) outlet structures. For example, a reservoir may have a spillway and several low-level outlet culverts. While there is an option to include gates on spillways, there is also an option to include a time-series of releases in addition to the uncontrolled releases from the various structures. An external analysis may be used to develop the additional releases based on an operations plan for the reservoir. When the main channel stage is low, water in the collection pond can drain through culverts into the main channel [26].

Figure 7 displays the flowchart but taking into consideration the existence of the reservoir Stronie Śląskie.

2.6. Computational Fluid Dynamics to Asses Reservoir Routing

To analyze the hydraulic capacity of the Stronie Śląskie reservoir that failed during the 2024 flood (and to compare the calculations with the hydrological model), an additional 3D numerical hydraulic model was developed to estimated the maximum hydraulic capacity during the extreme flood conditions (15 September 2024) when the reservoir collapsed. However, due to conflicts of interest with local Polish authorities, further research results cannot be published in this contribution. Therefore, the authors present the maximum capacity of the reservoir without the failure of the left earth dyke. The software Flow-3D version 12.0 was used for this purpose.

The 3D model was based on the modification of the continuity and momentum equations, namely, the commonly used Reynolds-average Navier–Stokes (RANS) equations. For the RANS technique, the mean velocity field may be defined by ensemble (time) averaging, which is represented via the following series of equations [34]:

$$\frac{\partial \bar{u}_i}{\partial t} + \bar{u}_j \frac{\partial \bar{u}_i}{\partial x_j} = -\frac{1}{\varrho}\frac{\partial \bar{p}}{\partial x_i} + \nu \frac{\partial^2 \bar{u}_i}{\partial x_j \partial x_j} - \frac{\partial}{\partial x_j} R_{ij} \tag{10}$$

$$\frac{\partial \bar{u}_i}{\partial x_i} = 0 \tag{11}$$

where $\bar{u}_i$ is the mean averaged velocity component, $\bar{p}$ is the mean pressure, ν is the molecular viscosity, ϱ is the water's density, and R_{ij} is the kinematic Reynolds stress tensor defined as (12)

$$R_{ij} = -\overline{u_i' u_j'} \tag{12}$$

where u_i' is the fluctuating part of the velocity.

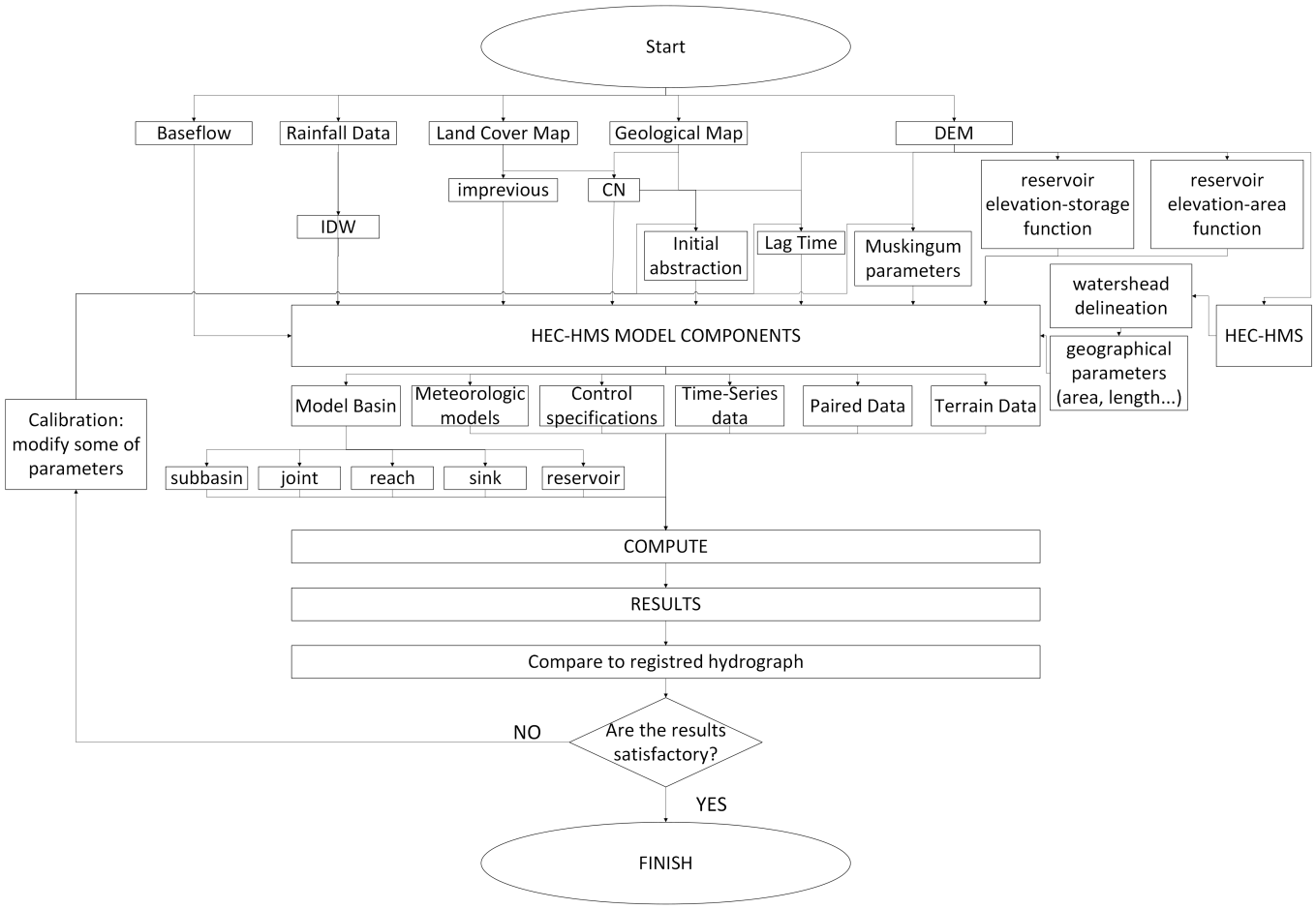


Figure 7. Flowchart displaying the modeling methodology used to calculate the flow hydrograph, including the reservoir.

Turbulence Closures-RANS

Eddy viscosity ν_T plays a profound role in turbulence modeling [35] and it is necessary to properly model the turbulent stresses (see Equation (12)) [35]. The Boussinesq approximation is a common method of computing turbulent stresses, and it is expressed as follows:

$$-\overline{u_i'u_j'} = \nu_T\left(\frac{\partial \bar{u}_i}{\partial x_j} + \frac{\partial \bar{u}_j}{\partial x_i}\right) - \frac{2}{3}k\delta_{ij} \tag{13}$$

where δ_{ij} is the Kronecker delta and k is the turbulent kinetic energy (TKE) per unit mass, which is defined as follows (14):

$$k \equiv \frac{1}{2}\overline{u_i'u_i'} \tag{14}$$

In the case of the $k-\varepsilon$ model, the eddy viscosity is calculated as follows:

$$\nu_T = c_\mu \frac{k^2}{\varepsilon} \tag{15}$$

and the TKE is modeled with the following equation:

$$\frac{\partial k}{\partial t} + \bar{u}_j\frac{\partial k}{\partial x_j} = \frac{\partial}{\partial x_j}\left(\nu + \frac{\nu_T}{\sigma_k}\frac{\partial k}{\partial x_j}\right) + P_k - \varepsilon \tag{16}$$

where P_k is the production of turbulence by shear, defined by

$$P_k = -\overline{u_i' u_j'} \frac{\partial \bar{u}_i}{\partial x_j} \tag{17}$$

and ε is the dissipation rate of k, modeled by

$$\frac{\partial \varepsilon}{\partial t} + \bar{u}_j \frac{\partial \varepsilon}{\partial x_j} = \frac{\partial}{\partial x_j}\left(\nu + \frac{\nu_T}{\sigma_\varepsilon}\frac{\partial \varepsilon}{\partial x_j}\right) + c_{\varepsilon 1}\frac{\varepsilon}{k}P_k - c_{\varepsilon 2}\frac{\varepsilon^2}{k} \tag{18}$$

The terms c_μ, σ_ε, $\sigma_{\varepsilon 1}$, and $\sigma_\varepsilon 2$ are the constants of the $k - \varepsilon$ model.

In the case of the RNG model, this turbulent closure is also part of the RANS technique, and it is based on the *k*-ε technique [36].

3. Hydrological Analysis

3.1. Models' Run and Calibration

Once all the geometric parameters, as well as hydrologic information, were retrieved [37], it was possible to run the model. The main issue at this stage is that the registered values at this gauge station present a gap of around 10 h, exactly when the second flood wave peak arose. Thus, the discrepancy between the model and the IMGW results is larger for the model output, but this remains in doubt because of lack the of registered information (between hours 95–105) at the Lądek-Zdrój gauge station [38].

Thus, the model was calibrated using the information of the flood that occured in the 2010 year (small flood wave), when the influence of the reservoir was not important during the flood event. The results of the model approaches and the registered values at the Lądek-Zdrój gauge station were satisfactory [38], which means that the model is more sensitive to the rainfall information than to the geographic data. The importance of the calibration process is to ensure the reliability of the model forecasts. Thus, once our model is calibrated, the simulation results become trustworthy [37].

After calibrating the original model and conducting the first simulations, the model was supplemented by simulating the functions of the Stronie Śląskie reservoir (located in sub-basin 3). The reservoir capacity was defined using Elevation–Storage–Area, introducing paired data from Elevation–Storage and Elevation–Area relationships. The data was obtained from the DEM using QGIS tools. The Stronie Śląskie Dam is composed of two bottom culverts, an intermediate arch-tunnel, and two upper spillways, as depicted in Figure 1. During the flood of September 2024, the height of the dam was additionally increased by sandbags provided by the local inhabitants of the town near the dam. The HEC-HMS programme encountered a problem related to the analysis of water flow through the reservoir due to such high rainfall that it was necessary to model the overflow of water over the dam crest (upper spillways). As mentioned in the introduction, the dam break was not analyzed in this case.

Figure 8 depicts the inflow hydrographs of each flood release component of the Stronie Śląskie reservoir dam during the September 2024 flood events (see Figure 1). The green line represents the water flow along the culverts of the structure, the light-blue line represents the hydrograph of the middle-arch tunnel, and the green line represents the discharge over the spillways of the structure using the IDW data. The total inflow hydrograph is represented with an orange line.

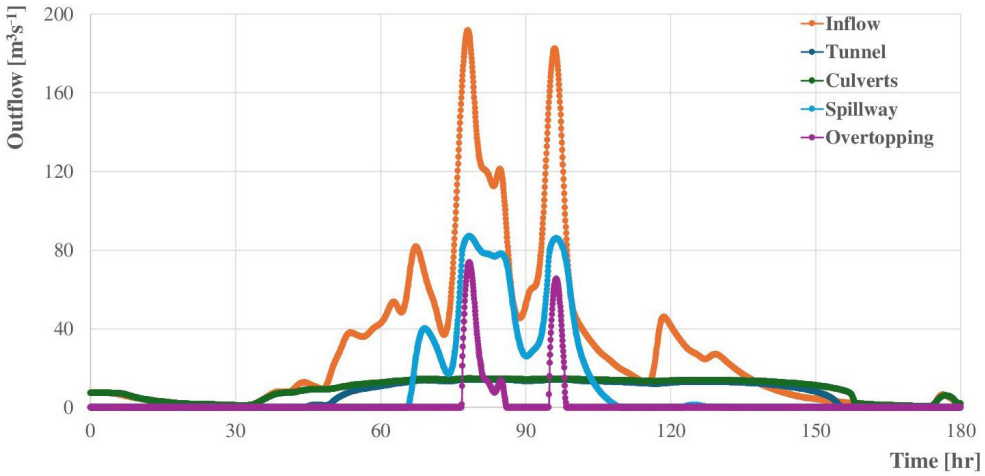


Figure 8. Estimated inflow hydrographs of the draining components of the reservoir.

This total inflow hydrograph was compared for both scenarios (see Figure 9). The hydrograph calculated using the data from the Śnieżnik meteorological station is depicted via a blue line and the hydrograph forecast from the IDW interpolation rainfall is depicted via a green line. As can be seen, both methodologies present good agreement. This confirms that the authors' model is reliable but sensitive to rainfall data. A sensibility analysis of the model will be included in future research.

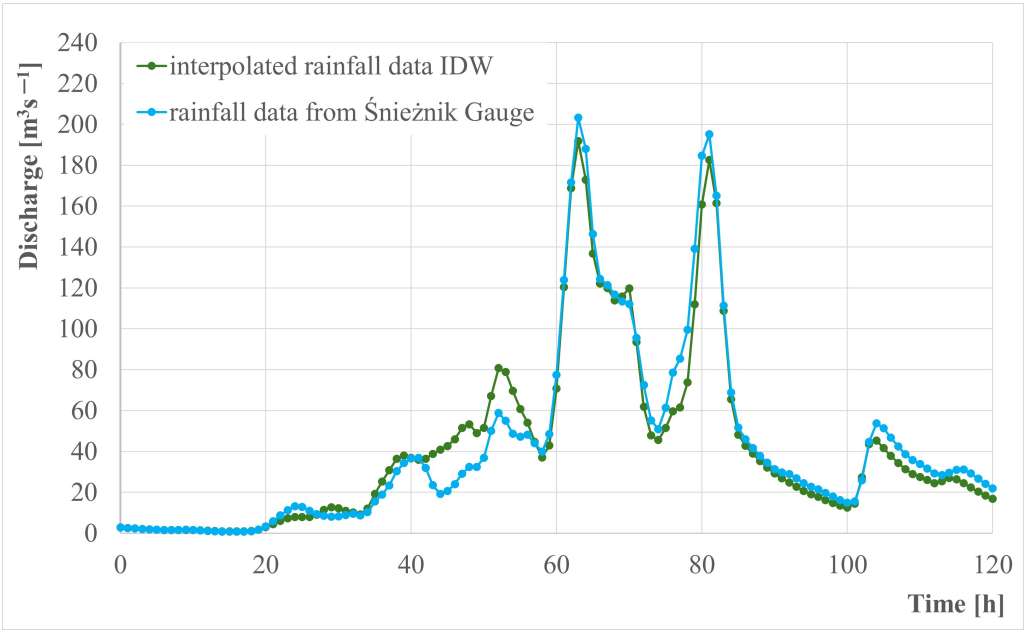


Figure 9. Comparison of inflow hydrographs of the Stronie Śląskie dam.

Figure 10 presents the outcomes of four simulation analyses (hydrographs) at the Lądek-Zdrój gauge section. Each of these hydrographs illustrates the registered flow rates at the Lądek-Zdrój station (dark blue line) and is compared with the model output for different scenarios using the IDW interpolated data and the data from the Śnieżnik meteorological station. The purple line represents the results of the simulations using the IDW data and considering the storage function of the reservoir. while the light-blue line represents the forecast flood wave considering the storage function but using the data from the Śnieżnik station. The green line represents the hydrograph without the reservoir using the IDW data, while the orange line represents the hydrograph using the data from Śnieżnik, also without the reservoir.

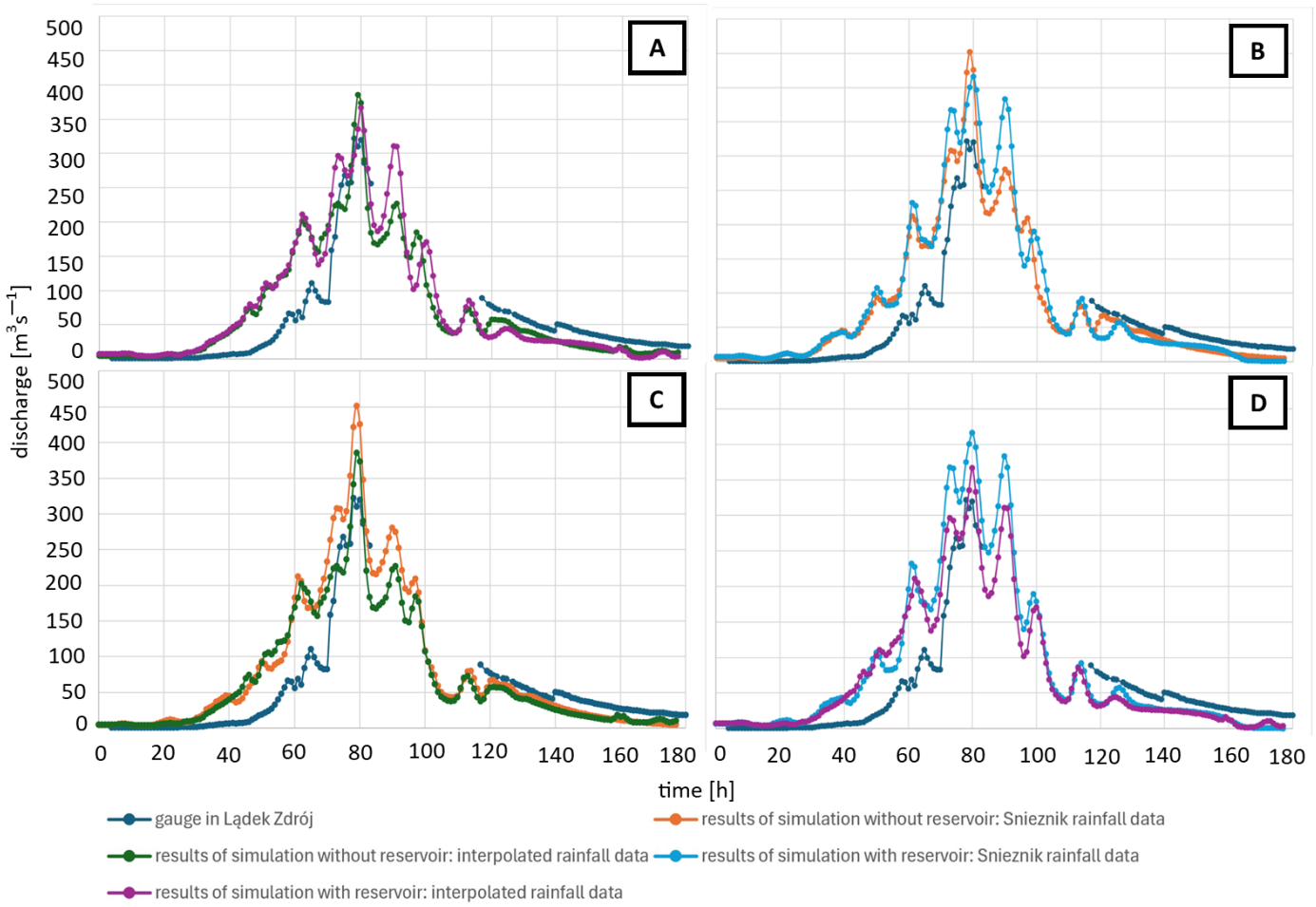


Figure 10. Comparison of hydrographs of the Lądek-Zdrój gauge cross-section.

Hydrographs A and B display the results from dual models (with the Stronie Śląskie reservoir and without). The difference between Figure 10A,B is that the implemented rainfall data series used the IDW for A and the information from the Śnieżnik gauge for B. The same situation is forecast for C and D but using the meteorological station data (C—without the reservoir; D—with the reservoir).

As can be seen, the model including the storage function of the reservoir using the IDW interpolated data most closely aligns with the highest peak when compared to the gauge registered data at Lądek-Zdrój. Prior to the maximal peak (around hour 80 of the simulation), significant discrepancies exist between the simulated results and the registered data (between hours 60 and 70). These discrepancies vary from 80 to 120 m^{3}s^{-1}. In this context, the model including the reservoir shows a better fit with the gauge data. In the interval, when recorded data is missing (85–115 h), all analyzed simulations depict three additional peaks with a gradual decrease. It is noteworthy that the first of these peaks is higher in the model with the reservoir, while the subsequent peaks are higher in the models without the reservoir. After the 115th hour, when recorded data resumes, the differences between these data and the simulation data are minimal.

3.2. Flood Routing at the Stronie Śląskie Reservoir Using CFD

A more detailed analysis of the maximal draining capacity of the reservoir can be carried out using CFD techniques. For this case study, the authors applied the Flow3D software v.12.0 developed by Flow Science. The graphical output of the model in 3D is depicted in Figure 11. The tiny lines show the border of the computational meshes that were used in the runs.

The 3D model offers data that are unattainable through the hydrological model, including the velocity components in three directions at each cell within the computational domain, the shear stresses on the dam walls, and the turbulence parameters. It also allows for fluid–structure interaction analysis [35]. However, this method comes with high computational costs, making it nearly incapable of analyzing an entire hydrological event.

A comparison between the estimation of the maximal draining capacity at the first floodwave peak is depicted in Table 4. As appreciated, the results present very good agreement. Due to the fact that there is no registered flow rate data at the moment of each event, an accurate analysis of errors cannot be carried out.

Table 4. Comparison of the maximal draining capacity of the reservoir outlet structures using HEC-HMS and Flow3D.

Outlet Element	Q-HMS (m^3s^{-1})	Q-CFD (m^3s^{-1})
Culverts	14.60	15.02
Mid-tunnel	14.27	14.78
Spillway	86.69	85.35

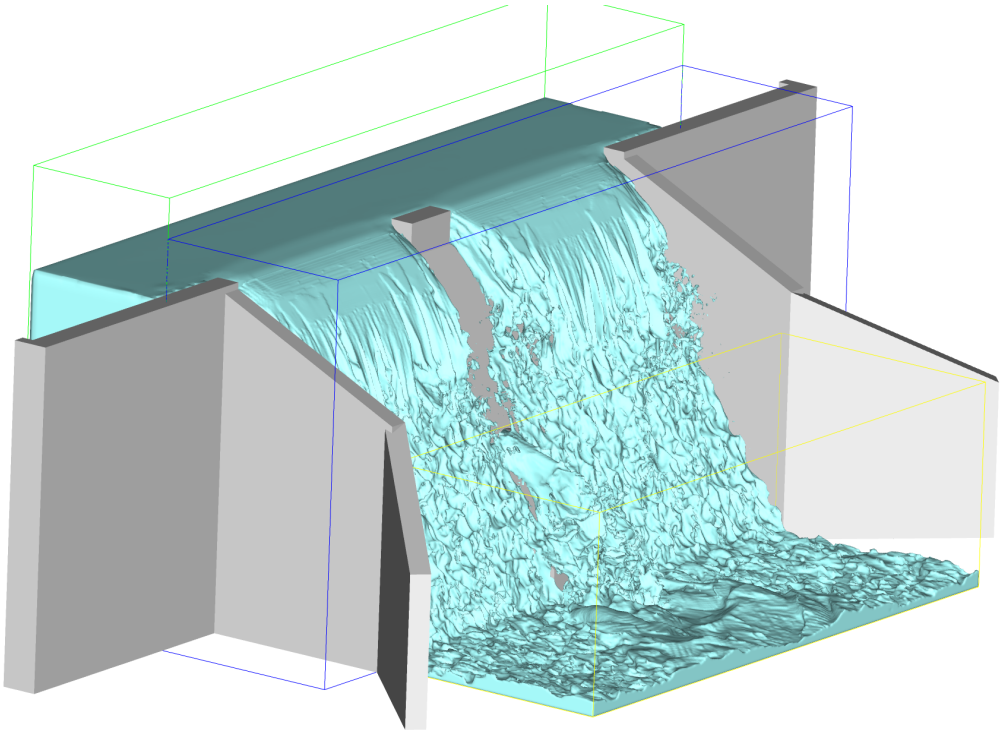


Figure 11. Axonometric view of the water flowing through the Stronie Śląskie dam at the highest reservoir elevation—15 September 2024.

4. Conclusions

In this study, the authors analyzed the September 2024 flood events at the Biała Lądecka Upper sub-basin and considered the influence of the Stronie Śląskie reservoir in the estimation of the flood wave hydrographs within the whole study area. It must be noted, however, that in this research, the catastrophe of the dam break of the left earth dyke was not included due to conflicts of interest at the moment of submitting this paper. Two modeling approaches were applied: (i) a hydrological model using the HEC-HMS 4.13 beta.6 software to analyze the meteorological event in full; and (ii) a CFD numerical approach to estimate the draining capacity considering the maximal registered elevation (at around noon of 15 September 2024).

It is important to remember that selecting the right parameters is essential in empirical hydrological modeling. Despite the use of some of the simpler methods in the rainfall-and model with only a few calibration parameters, the task remained complex; e.g., it was challenging to choose the correct travel time K in the Muskingum method. This parameter is dependent of the flow velocity, which, in turn, is influenced by varying water depths, which could affect the final results. Therefore, a calibration process is essential. The hydrological model was calibrated using previous data from a smaller flood event (no reservoir influence), which made the estimations reliable [38].

Based on the simulations and examining the hydrographs at the Lądek-Zdrój gauge station, it can be observed that applying the IDW precipitation data as an input leads to lower flow intensity hydrographs than the same hydrographs using the data from the Śnieżnik meteorological station (see Figure 10C,D). This could be a consequence of the higher rainfall values registered near the Śnieżnik station in September 2024.

Moreover, when comparing the simulated hydrographs at the gauge station location with the recorded data, it is evident that the scenario with the IDW interpolated data produced outcomes that were closer to the reality. Therefore, it is recommended to use interpolated data from different stations for modeling purposes, especially when analyzing the impact of man-made infrastructure (Figure 9). To decrease the uncertainty of the IDW methodology, an analysis of errors was performed.

The mean error (ME) was calculated for all analyzed data points (19). This measure can provide useful information as it is able to consider the direction of the errors. However, the results must be interpreted carefully, as the error values with different signs can cancel themselves out. The MAE, which is a popular error measure, is the average magnitude of errors in a set of predictions; it is defined by Equation (20) [39]:

$$ME = \frac{1}{n}\sum_{i=1}^{n}(zi_i - zs_i) \tag{19}$$

$$MAE = \frac{1}{n}\sum_{i=1}^{n}|zi_i - zs_i| \tag{20}$$

where n is a number of points, zi is the value obtained from interpolation, and zs is the value obtained from the meteorological station. It does not consider the direction of errors, given their average magnitude. In this method, all errors have equal weight. Furthermore, the root mean square error (RMSE) was calculated (21) [39].

$$RMSE = \sqrt{\frac{1}{n}\sum_{i=1}^{n}(zi_i - zs_i)^2} \tag{21}$$

RMSE is another popular error measure giving an absolute value, but due to the squaring of errors, it gives higher weight to larger errors. The RMSE is always larger than or equal to the MAE (RMSE = MAE when all errors have the same magnitude); the greater the difference between the RMSE and the MAE, the greater the variance of errors. Table 5 summarizes the analysis of errors of the seven IDW cases that were used in this study.

To analyze which parameter is more suitable to rainfall prediction, it is necessary to take into account the specific rainfall event. On the one hand, MAE is preferable for average prediction in the original units (i.e., mm of rain). It is also less influenced by rare rainfall errors; it tends to yield a more stable assessment of overall performance. On the other hand, RMSE's emphasis on larger errors is beneficial in these high-risk contexts. RMSE is also useful for model optimization as the RMSE aligns with the assumption of normally distributed errors and is mathematically convenient. The errors estimated by the RMSE are

approximately normal (often after transformation). Thus, model residuals are expected to follow a normal distribution, and RMSE is theoretically the optimal choice [40].

Table 5. Analysis of errors of the IDW method using different rainfall gauges, where BL is Bolesławów, OK is Ołdrzychowice Kłodzkie, KA is Kamienica, SG is Stary Gierałtów, SŚ is Stronie Śląskie, LZ is Lądek-Zdrój, and ŚN is Śnieżnik.

Cases of Analyzed Rainfall Data	ME	MAE	RMSE	ME	MAE	RMSE
	mean [mm]			max [mm]		
(A) All 7 rainfall stations	−0.132	0.902	1.095	−1.288	4.335	4.981
(B) 6 stations, excluding BL	−0.017	0.194	0.228	−0.162	1.885	2.151
(C) 6 stations, excluding OK	0.016	0.800	0.921	0.036	0.970	1.165
(D) 5 stations, excluding KA and SG	0.059	0.351	0.453	0.290	1.719	1.928
(E) 5 stations, excluding KA and OK	0.492	1.656	2.045	0.492	1.656	2.045
(F) 4 stations—SŚ, LZ, OK, and ŚN	−0.304	0.755	0.798	−0.678	1.598	1.701
(G) 4 stations—BL, SŚ, LZ, and ŚN	0.496	1.902	2.367	0.749	3.154	3.433
(H) 3 stations—-LZ, OK, and ŚN	0.047	0.134	0.167	0.122	0.250	0.340

As can be seen in Table 5, the largest error occurred when seven station were considered to forecast missing data (MAE and RMSE) in the hydrographs. Hence, the authors avoided using this interpolation when the missing values were at the beginning of the rainfall event and the seven stations were not representative; e.g., BL is located at the outlet of the basin, so case H was used as these rainfall stations are located in the higher parts of the catchment. Similar decisions were made at different time points in the simulation.

In the present analysis, the draining capacity of the dam outlet elements could be forecast (without considering the earth dam failure of the reservoir). As depicted in Figures 8 and 9, the model provides important information that can be used in future flood events for early warning, storage planning, and flood risk management; e.g., using this information, the decision-makers can propose changes in the actual structure's dimensions, taking into consideration the new hydrological conditions brought about by climate change. This can also be complemented by state-of-the-art techniques such as CFD (see Figure 11 and Table 4).

The advantage of using 3D numerical modeling is that, evidently, the results are more accurate. Nonetheless, the computational costs are considerably higher; e.g., the hydraulic routing analisis of the reservoir using HEC-HMS was carried out for more than 72 h and the computational time was nearly one minute (using a normal PC-intel7 processor); while calculating the hydraulic capacity of the structure in maximal conditions for a minute in real time was accomplished in 24 h using the same PC. Thus, 3D modeling approaches are still limited for commercial and engineering purposes.

In future analyses, the authors will consider the impact of the catastrophe on flood waves (i.e., via dam-break analyses). We also intend to employ other hydrological models, e.g., routing methods and new 2D hydraulic models, in the dam routing of the Stronie Śląskie dam, and to expand the case study study to the whole of the Biała Lądecka basin.

Author Contributions: Conceptualization, J.I. and O.H.-G.; methodology, J.I. and O.H.-G.; software, J.I. and O.H.-G.; formal analysis, O.H.-G. and J.I. investigation, O.H.-G. and J.I.; writing—original draft preparation, O.H.-G. and J.I.; supervision, O.H.-G. All authors have read and agreed to the published version of the manuscript.

Funding: This research received no external funding.

Data Availability Statement: The data used in this study was retrieved from different online services such as https://www.geoportal.gov.pl (accessed on 21 October 2024) for DEM acquisition; https://scalgo.com/live/poland (accessed on 21 October 2024) for information about land-cover;

https://danepubliczne.imgw.pl/ (accessed on 14 October 2024) for meteorological data; and https://www.pgi.gov.pl (accessed on 28 October 2024) for data concerning the geological information. Due to the fact that people from our institution (Wrocław University of Science and Technology) are currently carrying out an investigation of the causes of the Stronie Śląskie reservoir catastrophe, the authors are unable to provide the results of the modeling output for the influence of this flood mitigation infrastructure. However, it will be included in future research.

Conflicts of Interest: The authors declare no conflicts of interest.

Abbreviations

The following abbreviations are used in this manuscript:

CFD	Computational Fluid Dynamics
CN	Curve Number
DEM	Digital Elevation Model
GIS	Geographical Information Systems
HEC	Hydrologic Engineering Center
HMS	Hydrologic Modeling System
IDW	Inverse Distance Weighted
IMGW	Polish Institute of Meteorology and Water Management (Polish language acronym)
NMT	Numerical Model of the Terrain
PIB	Polish Geological Institute (Polish language acronym)
RANS	Reynolds-Averaged Navier–Stokes
RNG	RANS Renormalized Group
SCS	Soil Conservation Service

References

1. Kundzewicz, Z.W.; Januchta-Szostak, A.; Nachlik, E.; Pińskwar, I.; Zaleski, J. Challenges for Flood Risk Reduction in Poland's Changing Climate. *Water* **2023**, *15*, 2912. [CrossRef]
2. Flood in Poland, September 2024. Available online: https://pck.pl/en/co-robimy/powodz-2024 (accessed on 10 December 2025).
3. Kumari, M.; Diksha; Kalita, P.; Mishra, V.N.; Choudhary, A.; Abdo, H.G. Rainfall-runoff modelling using GIS based SCS-CN method in umiam catchment region, Meghalaya, India. *Phys. Chem. Earth Parts A/B/C* **2024**, *135*, 103634. [CrossRef]
4. Chen, F.W.; Liu, C.W. Estimation of the Spatial Rainfall Distribution using Inverse Distance Weighting (IDW) in the Middle of Taiwan. *Paddy Water Environ.* **2012**, *10*, 209–222. [CrossRef]
5. Chutsagulprom, N.; Chaisee, K.; Wongsaijai, B.; Inkeaw, P.; Oonariya, C. Spatial interpolation methods for estimating monthly rainfall distribution in Thailand. *Theor. Appl. Climatol.* **2022**, *148*, 317–328. [CrossRef]
6. Sitterson, J.; Knightes, C.D.; Parmar, R.; Wolfe, K.; Avant, B.; Muche, M.E. An Overview of Rainfall-Runoff Model Types. In Proceedings of the International Congress on Environmental Modelling and Software, Fort Collins, CO, USA, 24–28 June 2018.
7. Green, W.H.; Ampt, G.A. Studies on Soil Phyics. *J. Agric. Sci.* **1911**, *4*, 1–24. [CrossRef]
8. Ahuja, L.; Ross, J. A new Green-Ampt model for infiltration through a surface seal permitting transient parameters below the seal. In Proceedings of the National Conference on Advances in Infiltration, Chicago, IL, USA, 12–13 December 1983.
9. Barry, D.A.; Parlange, J.Y.; Li, L.; Jeng, D.S.; Crapper, M. Green–Ampt approximations. *Adv. Water Resour.* **2005**, *28*, 1003–1009. [CrossRef]
10. Basha, H. Infiltration models for semi-infinite soil profiles. *Water Resour. Res.* **2011**, *47*. [CrossRef]
11. Bouwer, H. *Groundwater Hydrology*; McGraw-Hill: New York, NY, USA, 1978.
12. Chen, L.; Young, M.H. Green-Ampt infiltration model for sloping surfaces. *Water Resour. Res.* **2006**, *42*. [CrossRef]
13. Gowdish, L.; Muñoz-Carpena, R. An improved Green–Ampt infiltration and redistribution method for uneven multistorm series. *Vadose Zone J.* **2009**, *8*, 470–479. [CrossRef]
14. Hilpert, M.; Glantz, R. Exploring the parameter space of the Green–Ampt model. *Adv. Water Resour.* **2013**, *53*, 225–230. [CrossRef]
15. Hogarth, W.; Lockington, D.A.; Barry, D.A.; Parlange, M.; Haverkamp, R.; Parlange, J.Y. Infiltration in soils with a saturated surface. *Water Resour. Res.* **2013**, *49*, 2683–2688. [CrossRef]
16. Mein, R.G.; Larson, C.L. Modeling infiltration during a steady rain. *Water Resour. Res.* **1973**, *9*, 384–394. [CrossRef]
17. Parlange, J.Y.; Lisle, I.; Braddock, R.; Smith, R. The three-parameter infiltration equation. *Soil Sci.* **1982**, *133*, 337–341. [CrossRef]
18. Voller, V.R. On a fractional derivative form of the Green–Ampt infiltration model. *Adv. Water Resour.* **2011**, *34*, 257–262. [CrossRef]

19. Chen, L.; Xiang, L.; Young, M.H.; Yin, J.; Yu, Z.; van Genuchten, M.T. Optimal parameters for the Green-Ampt infiltration model under rainfall conditions. *J. Hydrol. Hydromech.* **2015**, *63*, 93–101. [CrossRef]
20. Mockus, V. Estimation of total (and peak rates of) surface runoff for individual storms. In *Exhibit A of Appendix B, Interim Survey Report Grand (Neosho) River Watershed, USDA*; U.S. Department of Agriculture (USDA): Washington, DC, USA, 1949; Volume 1.
21. Sherman, L. The unit hydrograph method. In *Physics of the Earth*; Meinzer, O.E., Ed.; Dover Publications, Inc.: New York, NY, USA, 1949; pp. 514–525.
22. Andrews, R. *The Use of Relative Infiltration Indices in Computing Runoff*; Unpublished; Soil Conservation Service: Fort Worth, TX, USA, 1954; Volume 6.
23. Ogrosky, H. *Service Objectives in the Field of Hydrology*; Unpublished; Soil Conservation Service: Lincoln, NE, USA, 1956; Volume 5.
24. Mishra, S.; Singh, V. *Soil Conservation Service Curve Number (SCS-CN) Methodology*; Springer Nature: Dordrecht, The Netherlands, 2013.
25. Caletka, M.; Šulc Michalková, M.; Karásek, P.; Fučík, P. Improvement of SCS-CN Initial Abstraction Coefficient in the Czech Republic: A Study of Five Catchments. *Water* **2020**, *12*, 1964. [CrossRef]
26. U.S. Army Corps of Engineers. HEC-HMS: Hydrologic Modeling System. 2018. Available online: https://www.hec.usace.army.mil/software/hec-hms/ (accessed on 15 July 2024).
27. Dixon, B.; Uddameri, V. Watershed Delineation. In *GIS and Geocomputation for Water Resource Science and Engineering*; John Wiley & Sons, Ltd.: Hoboken, NJ, USA, 2015; Chapter 20, pp. 297–312. [CrossRef]
28. SCALGO. SCALGO Live Documentation. 2024. Available online: https://scalgo.com/en-US/scalgo-live-documentation/about/support (accessed on 21 August 2024).
29. Cheng, X.; Ma, X.; Wang, W.; Xiao, Y.; Wang, Q.; Liu, X. Application of HEC-HMS Parameter Regionalization in Small Watershed of Hilly Area. *Water Resour. Manag.* **2021**, *35*, 1961–1976. [CrossRef]
30. IMGW. Meteo IMGW-PIB. 2025. Available online: https://meteo.imgw.pl/ (accessed on 14 August 2024).
31. Bedient, P.B.; Huber, W.C. *Hydrology and Floodplain Analysis*; Addison-Wesley: Reading, MA, USA, 1992.
32. Burrough, P.; McDonnell, R. *Principles of Geographical Information Systems*; Oxford University Press: Oxford, UK, 1998.
33. Goovaerts, P. Geostatistical approaches for incorporating elevation into the spatial interpolation of rainfall. *J. Hydrol.* **2000**, *228*, 113–129. [CrossRef]
34. Wu, W. *Computational River Dynamics*; Taylor & Francis: Abingdon, UK, 2007. [CrossRef]
35. Herrera-Granados, O.; Kostecki, S. Numerical and physical modeling of water flow over the ogee weir of the new Niedów barrage. *J. Hydrol. Hydrodyn.* **2016**, *64*, 67–74. [CrossRef]
36. Herrera-Granados, O. Numerical Analysis of Flow Behavior in a Rectangular Channel with Submerged Weirs. *Water* **2021**, *13*, 1396. [CrossRef]
37. Herrera-Granados, O. Chapter 19-Theoretical background and application of numerical modeling to surface water resources. In *Water Resource Modeling and Computational Technologies*; Zakwan, M., Wahid, A., Niazkar, M., Chatterjee, U., Eds.; Elsevier: Amsterdam, The Netherlands, 2022; Current Directions in Water Scarcity Research; Volume 7, pp. 319–340. [CrossRef]
38. Izydorski, J.; Herrera-Granados, O. *Analisys of the 2024 Flood Events in the Upper Biała Lądecka Basin up to the Lądek Zdrój Town (In Production)*; Springer: Berlin/Heidelberg, Germany, 2026; pp. 1–2.
39. Uciechowska-Grakowicz, A.; Herrera-Granados, O. Riverbed Mapping with the Usage of Deterministic and Geo-Statistical Interpolation Methods: The Odra River Case Study. *Remote Sens.* **2021**, *13*, 4236. [CrossRef]
40. Khoshvaght, H.; Permala, R.R.; Razmjou, A.; Khiadani, M. A critical review on selecting performance evaluation metrics for supervised machine learning models in wastewater quality prediction. *J. Environ. Chem. Eng.* **2025**, *13*, 119675. [CrossRef]

Disclaimer/Publisher's Note: The statements, opinions and data contained in all publications are solely those of the individual author(s) and contributor(s) and not of MDPI and/or the editor(s). MDPI and/or the editor(s) disclaim responsibility for any injury to people or property resulting from any ideas, methods, instructions or products referred to in the content.